

OPEN

[¹⁸F]fluorothymidine and [¹⁸F]fluorodeoxyglucose PET Imaging Demonstrates Uptake and Differentiates Growth in Neurofibromatosis 2 Related Vestibular Schwannoma

*†Jose M. Anton-Rodriguez, *‡Daniel Lewis, §Ibrahim Djoukhar, ||David Russell, *†Peter Julyan, *‡David Coope, ‡Andrew T. King, ‡Simon K. L. Lloyd, ¶D. Gareth Evans, *#Alan Jackson, and *#Julian C. Matthews

*Division of Informatics, Imaging and Data Sciences, MAHSC, University of Manchester; †Christie Medical Physics and Engineering, The Christie NHS Foundation Trust, Manchester; ‡Manchester Skull Base Unit, Manchester Centre for Clinical Neurosciences, Manchester Academic Health Science Centre, Salford Royal NHS Foundation Trust; §Department of Neuroradiology, Manchester Centre for Clinical Neurosciences, Salford Royal NHS Foundation Trust, Manchester Academic Health Science Centre; ||Department of Radiology, Manchester University NHS Foundation Trust; ¶Manchester Centre for Genomic Medicine, St Mary's Hospital, Manchester University Hospitals National Health Service Foundation Trust and Manchester Academic Health Science Centre, Manchester, UK; and #Division of Neuroscience and Experimental Psychology, School of Biological Sciences, Faculty of Biology, Medicine and Health, Manchester Academic Health Science Centre (MAHSC), University of Manchester

Objective: To investigate whether [¹⁸F]fluorothymidine (FLT) and/or [¹⁸F]fluorodeoxyglucose (FDG) positron emission tomography (PET) can differentiate growth in neurofibromatosis 2 (NF2) related vestibular schwannomas (VS) and to evaluate the importance of PET scanner spatial resolution on measured tumor uptake.

Methods: Six NF2 patients with 11 VS (4 rapidly growing, 7 indolent), were scanned with FLT and FDG using a high-resolution research tomograph (HRRT, Siemens) and a Siemens Biograph TrueV PET-CT, with and without resolution modeling image reconstruction. Mean, maximum, and peak standardised uptake values (SUV) for each tumor were derived and the intertumor correlation between FDG and FLT uptake was compared. The ability of FDG and FLT SUV values to discriminate between rapidly growing and slow growing (indolent) tumors was assessed using receiver operator characteristic (ROC) analysis.

Results: Tumor uptake was seen with both tracers, using both scanners, with and without resolution modeling. FDG

and FLT uptake was correlated ($R^2 = 0.67-0.86$, $p < 0.01$) and rapidly growing tumors displayed significantly higher uptake (SUV_{mean} and SUV_{peak}) of both tracers ($p < 0.05$, one tailed t test). All of the PET analyses performed demonstrated better discriminatory power (AUC_{ROC} range = 0.71–0.86) than tumor size alone ($AUC_{ROC} = 0.61$). The use of standard resolution scanner with standard reconstruction did not result in a notable deterioration of discrimination accuracy.

Conclusion: NF2 related VS demonstrate uptake of both FLT and FDG, which is significantly increased in rapidly growing tumors. A short static FDG PET scan with standard clinical resolution and reconstruction can provide relevant information on tumor growth to aid clinical decision making. **Key Words:** [¹⁸F]fluorodeoxyglucose (FDG)—[¹⁸F]fluorothymidine (FLT)—Neurofibromatosis 2—PET—Vestibular schwannoma.

Otol Neurotol 40:826–835, 2019.

Address correspondence and reprint requests to Jose M. Anton-Rodriguez, Ph.D., Wolfson Molecular Imaging Centre, 27 Palatine Road, Withington, Manchester, M20 3LJ, UK; E-mail: jose.anton@manchester.ac.uk

This work is supported by Cancer Research UK and the Engineering and Physical Sciences Research Council Cancer Imaging Centre in Cambridge and Manchester (C8742/A18097).

J.M.A.-R. was undertaking a PhD supported by The Christie NHS Foundation Trust and The University of Manchester. D.G.E. is an NIHR Senior Investigator supported by the Biomedical Research Centre, Manchester (NIHR programme IS-BRC-1215-20007).

The authors disclose no conflicts of interest.

Supplemental digital content is available in the text.

This is an open access article distributed under the terms of the Creative Commons Attribution-Non Commercial-No Derivatives License 4.0 (CCBY-NC-ND), where it is permissible to download and share the work provided it is properly cited. The work cannot be changed in any way or used commercially without permission from the journal.

DOI: 10.1097/MAO.0000000000002272

Neurofibromatosis 2 (NF2) is a dominantly inherited tumor predisposition syndrome affecting approximately 1 in 33,000 live births (1). The hallmark of this condition is the development of bilateral vestibular schwannomas (VS) (2,3) and once diagnosed patients typically undergo annual magnetic resonance imaging (MRI) screening to evaluate the size and growth with a cohort of tumors displaying relatively rapid growth (3,4). The cornerstone of modern NF2 management is conservation of hearing function and quality of life (3,5). While surgery plays a role in the management of rapidly growing tumors, the decision to operate depends on multiple factors including hearing deterioration rate, tumor growth rate, and tumor size (3). Surgery carries significant risks such as facial nerve injury (3), but early surgery, before tumors become too large, reduces the complication risk, and improves the outcome of adjunctive hearing preservation techniques such as auditory brainstem implantation (3,6–9). There is therefore a clinical need to identify rapidly growing VS early but with current MRI screening regimens there is a danger of missing significant growth due to the time-interval between scans. Furthermore, the accuracy and interobserver reproducibility of tumor measurements varies considerably depending on the measurement method used (10,11) and there is considerable debate within the literature as to what constitutes significant growth within lesions (12). An imaging biomarker that allows earlier identification of rapidly growing tumors would therefore be of clinical utility, particularly to patients harboring tumors that are approaching the threshold size for increased surgical risk. In these cases detecting further growth through serial MRI may mean that the optimum window for management has been missed whereas predicting growth offers the best opportunity to maximize surgical outcomes, patient quality of life, and avoid resulting costly treatment (13).

The positron emission tomography (PET) tracers fluorine-18 labeled deoxy-2-D-glucose (FDG) and 3'-deoxy-3'-fluorothymidine (FLT) have been increasingly used in oncology as imaging biomarkers of cellular metabolism and cellular proliferation respectively. Tumor cells preferentially accumulate FDG due to increased expression of glucose membrane transporters and the enzyme hexokinase, alongside a tendency to favor the more inefficient anaerobic pathway resulting in greater metabolic demand (Warburg effect) (14–18). FLT is transported into cells by the same nucleoside transporters as thymidine, and undergoes intracellular phosphorylation through the enzyme thymidine kinase 1. Elevation of thymidine kinase 1 occurs in rapidly dividing cells and consequently FLT uptake is a marker of cellular proliferation rate (19). Whereas FDG use within the central nervous system has been limited due to constitutively high uptake within the normal brain (20,21), brain uptake of FLT is normally limited by the blood–brain barrier (22,23), but has been demonstrated in regions of blood–brain barrier disruption such as within intrinsic glioma (24,25).

PET imaging in VS can be challenging and previous FDG PET studies in non-NF2 patients with sporadic

tumors have shown inconclusive results due to low uptake within the tumor compared with the adjacent cerebellum (20,21). Similarly inconclusive results have been reported when using other PET tracers relevant to central nervous system tumors such as [¹¹C]methionine (20). FLT or FDG-PET has not, however, been previously described in NF2 patients, and there is growing evidence that sporadic and NF2 related tumors are biologically different both at the macroscopic level (26), but also with regard to their cellular proliferation indices (27,28).

The rationale of this pilot study was to investigate whether PET with FLT and/or FDG in combination with MR could be used in the future to assist in refining clinical decision making in NF2 related VS. The objective of this study was to therefore first assess if VS in a cohort of NF2 patients have measurable FLT and/or FDG uptake, and second to determine if rapidly growing tumors displayed differences in the uptake of these PET tracers compared with more indolent tumors. Given the comparatively small size and technically challenging location of VS in the context of PET imaging, a novel study design was adopted by which patients were scanned using both a conventional PET-CT and a high-resolution research tomograph (HRRT), which has the highest spatial resolution for human brain PET (29). Through such an approach the effect of scanner spatial resolution and reconstruction methods on tracer uptake could also be assessed.

METHODS

Patients

Patients were recruited via the nationally commissioned, specialized NF2 multidisciplinary team meeting in Manchester, UK. Adult patients (aged between 18 and 70 yr of age) with a confirmed diagnosis of NF2 and at least one vestibular schwannoma (VS) were recruited. Exclusion criteria included: female patients pregnant or intending to become pregnant; patients who had undergone previous radiotherapy or antiangiogenic treatment; and patients with contra-indications to MRI. All patients gave informed written consent. The study was approved by an independent research ethics committee (REC 13/NW/0260) and by the United Kingdom Administration of Radioactive Substances Advisory Committee (ARSAC RPC 595/3586/30119).

All patients had undergone previous routine clinical assessment including MRI at 6 to 12 month intervals and the median length of follow-up across all patients was 1.52 years (range = 0.60–7.30 yr). The study MRI scan was reviewed in addition to the results of previous clinical MR imaging by the multidisciplinary team and tumors were classified as either rapidly growing or indolent. This classification reflected clinical decision making in these patients with tumors being classified as indolent undergoing further radiological surveillance and rapidly growing tumors being considered for either surgical resection or treatment with the antiangiogenic agent bevacuzimab (Avastin). To confirm the differential growth pattern across these two cohorts, volumetric measurements of tumor size were made for the preceding clinical scan, the study MR scan, and a follow-up scan 1 year later (see Table 1). Volumetric measurements were made on T₁-weighted (T1W) postcontrast imaging using the semiautomatic segmentation tool within the Brainlab iPlan software (Brainlab AG Germany) and the results

TABLE 1. Patient demographics, tumor features, and clinical outcome at 1-year follow-up

Patient	Location	Patient Age ^c and Sex	Growth Classification	Volume on Preceding Clinical Scan (cm ³)	Volume at Time of PET Scan (cm ³)	Volume 1 Yr Following PET Scan (cm ³)	Annual Adjusted Volume Change (cm ³ /yr)	Status of VS 1 Yr Following the PET Scan
A	Right	33 Female	RG	0.29	0.36 ^a	Resected	0.09	Resected—cochlear preserving surgery
	Left		RG	1.36	1.60	2.09	0.43	Continued growth. Patient qualified for Bevacizumab treatment.
B	Right	48 Male	Indolent	0.95	0.84	0.87	-0.04	Monitoring
	Left		Indolent	2.22	2.23	2.30	0.04	Monitoring
C ^b	Right	32 Male	Indolent	0.85	0.79 ^a	0.82	-0.02	Monitoring.
D	Right	21 Female	RG	1.34	1.42	3.30	0.99	Continued growth. Patient qualified for Bevacizumab treatment.
	Left		Indolent	0.22	0.23 ^a	0.28	0.03	Monitoring
E	Right	59 Male	RG	0.24	0.67 ^a	Resected	0.46	Resected- cochlear preserving surgery
	Left		Indolent	0.04	0.07 ^a	0.07	0.02	Monitoring
F	Right	55 Female	Indolent	Very small enhancing intracanalicular nodule			N/A	Monitoring
	Left		Indolent	0.26	0.23 ^a	0.20	-0.03	Monitoring

^aIntracanalicular lesion at the time of PET scan.

^bPatient C had a large left VS removed 1 year before study.

^cAge at the time the PET scans took place.

RG indicates rapid growing.

of segmentation were reviewed and, where necessary, edited by an experienced neuroradiologist (I.D.).

PET Data Acquisition

Patients were scanned using FDG and FLT on two separate occasions, less than a week apart. For both tracers 200 MBq was the target injected activity. Patients were scanned using both a conventional PET-CT scanner, the Truepoint TrueV Biograph PET-CT scanner (Siemens), with a spatial resolution of approximately 4.5 mm full width at half maximum (30); and with a brain dedicated scanner the HRRT, (Siemens) with spatial resolution of approximately 2.5 mm full width at half maximum (29). For each radiotracer, the scan sequence followed a 60-gap-30-gap-30 minute structure with alternated order of scanners, i.e., three scans for each radiotracer injection alternating between the PET-CT and the HRRT (with sequence shown in supplementary Figure 1C, <http://links.lww.com/MAO/A784>). Patients were placed on one of the two scanners (with the initial scanner altering between patients), injected with the radiotracer, and data acquired for 60 minutes (scan 1). Following a short break of between 10 and 20 minutes, patients were placed on the other scanner, with data acquired for 30 minutes (scan 2). Finally, following a second short break the patient was placed on the original scanner with data acquired for a further 30 minutes (scan 3).

This scan sequence was devised to allow assessment of tracer uptake during scan 2 at approximately 75 minutes postinjection on both scanners, either from direct measurement or from linear interpolation of data from scans 1 and 3 (radioactivity concentrations on the VS followed an approximately linear relationship during this period for both tracers). For attenuation correction, a 6-minute transmission scan was acquired when

using the HRRT (preinjection for scan 1 and postemission acquisition for scans 2 and 3) and a pre-emission CT scan when using the TrueV PET/CT scanner.

Image Reconstruction

Data from both scanners were reconstructed using implementations of three-dimensional iterative Ordinary Poisson Ordered Subset Expectation Maximisation (31) without (No-RM) and with resolution modeling (RM), reconstructing the data during the last 30 minutes of scan 1 and the data for scans 2 and 3, each into three 10 minute frames. For the TrueV scanner, the Siemens offline reconstruction package “e7_tools” was used with an image zoom of two resulting in images with a voxel size of 1.33 mm × 1.33 mm × 2.03 mm and an image grid dimension of 256 × 256 × 107 voxels. HRRT data was reconstructed using HRRT user community software generating images consisting of 256 × 256 × 207 voxels each of size 1.22 mm × 1.22 mm × 1.22 mm. In both cases, 10 and 12 iterations for No-RM and for RM respectively were conducted using 16 subsets for HRRT and 21 for the TrueV. RM reconstruction is referred to as HD for the TrueV PET (32) while for the HRRT user community software was used (33). The iterations and subsets selected reflect our standard image reconstruction protocols. Postreconstruction smoothing using Gaussian filters, which can be used to reduce image noise, was not performed since it could worsen image resolution, which was considered to be critical for this clinical application.

Reconstructions for both scanners were performed with full corrections including scatter and attenuation. In the case of HRRT, attenuation correction was calculated from a reconstructed and segmented μ -map image using the total variation TXTV method (34). To minimize the effects of patient motion

particularly the deterioration of image resolution, image-based motion correction using frame-by-frame realignment for each 10 minute frame was used for both scanners (35).

Delineation of Tumor VOI for PET Quantification

Tumor volumes of interest (VOI) for PET analysis were manually drawn on contrast enhanced T1W MR images (voxel size 0.9 mm × 0.9 mm × 0.8 mm), acquired as part of the study MRI. Regions were drawn to the edge of the enhancing tumor (care was taken when delineating the tumor to avoid partial volume effects from nearby structures or surrounding CSF) and subsequently were modestly eroded using a single iteration and a 3 × 3 × 1 erosion kernel. All manual outlining was done using Analyze version 11 and was performed under the supervision of AJ and ID, consultant neuroradiologists with over 40 years of combined experience. The study MRI was acquired on the same day as one of the PET scans for all the patients and therefore within 1 week of both PET scans. Using SPM 8 (<http://www.fil.ion.ucl.ac.uk/spm>), contrast enhanced T1W MRIs were coregistered to the 30 minutes motion corrected PET images from each of the three scans, and the manually drawn VOIs were resliced to PET space using the rigid body transformations calculated from this coregistration and nearest-neighbor interpolation.

PET quantification was performed using the standardized uptake value (SUV), whereby the radiotracer concentration at 75 minutes posttracer injection within each voxel was normalized by the injected radioactivity dose and patient weight (36). The tumor VOIs were then applied to the PET data to calculate SUV_{mean} (reflecting the overall regional tracer distribution), SUV_{max} (max value of the tracer distribution), and SUV_{peak} within each tumor. The latter is considered to be less sensitive to the VOI boundary and the uptake distribution (37).

Statistical Analysis

SPSS version 23 was used for all statistical analyses. The normality and homogeneity of variance for derived values was assessed using the Shapiro–Wilk and Levene test respectively. Intergroup differences in growth rate, SUV_{mean} , SUV_{max} , and SUV_{peak} between indolent and growing tumors were compared using a Student's *t* test. Linear regression analysis was undertaken to assess intertumor relationship between standardized uptake values for both FDG and FLT using each scanner with and without RM. Finally, the ability of each tracer to classify VS as rapidly growing was assessed using the area under the curve (AUC) of the receiver operator characteristic (ROC) curve for each SUV parameter, using the multidisciplinary defined growth classification as the truth.

RESULTS

Patient Demographics

Six patients with NF2 participated in this study, three males and three females with an age range of 21 to 59 years. Five patients had bilateral VS with the remaining patient having undergone previous surgical removal of a left-sided VS. Six tumors were intracanalicular at the time of the PET study and among the 11 VS, 4 were classified as rapidly growing while the rest were indolent (see Table 1). Confirmatory measurements of tumor volume change between the preceding clinical MRI and the study MRI demonstrated that compared with the indolent tumor group rapidly growing tumors displayed a higher annual adjusted growth rate (0.00 versus 0.49 cm³/yr, $p = 0.01$, two-tailed

t test). Patient demographics, tumor growth pattern, and the clinical outcome for each VS at 1-year follow-up are shown in Table 1. Mean injected tracer activities were 203 ± 2 MBq (range 202–210) of FLT and 206 ± 4 MBq (range 201–211) of FDG.

Visual Inspection of Uptake

Uptake of both FDG and FLT was seen in all tumors, using both scanners with and without RM. SUV mean, maximum, and peak of both tracers at approximately 75 to 105 minutes after injection are shown for the TrueV scanner in supplementary Tables 1C and 2C, <http://links.lww.com/MAO/A785>; and for the HRRT scanner in supplementary Tables 3C and 4C, <http://links.lww.com/MAO/A785>.

Figure 1 shows axial coregistered T₁-weighted contrast enhanced MRI, FDG PET, and FLT PET image sections for two patients (A and D) with bilateral tumors. All of the PET images shown were acquired using the TrueV scanner and show decay corrected SUV (g/ml) at approximately 75 to 105 minutes postinjection with the FDG images windowed to saturate the high brain uptake. Patient A (top row) had bilateral rapidly growing tumors, with the right smaller VS scheduled for surgical removal at the time of the PET scans. High uptake of both tracers is observed in the larger left-sided VS, with a small area of focal FDG uptake within the right-sided tumor. Patient D (bottom row) also had bilateral VS, with the right-sided tumor classified as rapidly growing and the left-sided tumor classified as slow growing (indolent). For both tracers clear uptake is observed for the right-sided rapidly growing tumor while little uptake is observed for the left-sided tumor.

Group Comparison

Intergroup differences in tumor SUV_{mean} , SUV_{max} , and SUV_{peak} between rapidly growing and indolent tumors for both FDG and FLT are shown in Table 2. The group comparison between FDG and FLT for both scanners using RM is presented in Figure 2. Rapidly growing tumors displayed significantly higher FDG SUV_{mean} and SUV_{peak} compared with indolent tumors using both scanners, with and without RM ($p < 0.05$, one-tailed *t* test). With the exception of values derived using the HRRT scanner without RM, the FDG SUV_{max} values were also significantly higher in the rapidly growing tumor group ($p < 0.05$).

While use of the TrueV scanner without RM did not demonstrate a significant difference in FLT uptake between rapidly growing and indolent tumors ($p > 0.05$), use of the TrueV with RM did demonstrate significantly higher FLT SUV_{mean} values in the rapidly growing tumors ($p < 0.05$, one-tailed *t* test). Similarly, use of the HRRT scanner with and without RM also demonstrated significantly higher SUV_{mean} and SUV_{peak} values compared with indolent tumors ($p < 0.05$, one-tailed *t* test).

Scatter Plots

Scatter plots of SUV for FDG against FLT for the TrueV and HRRT scanners are shown in Figure 3. Each

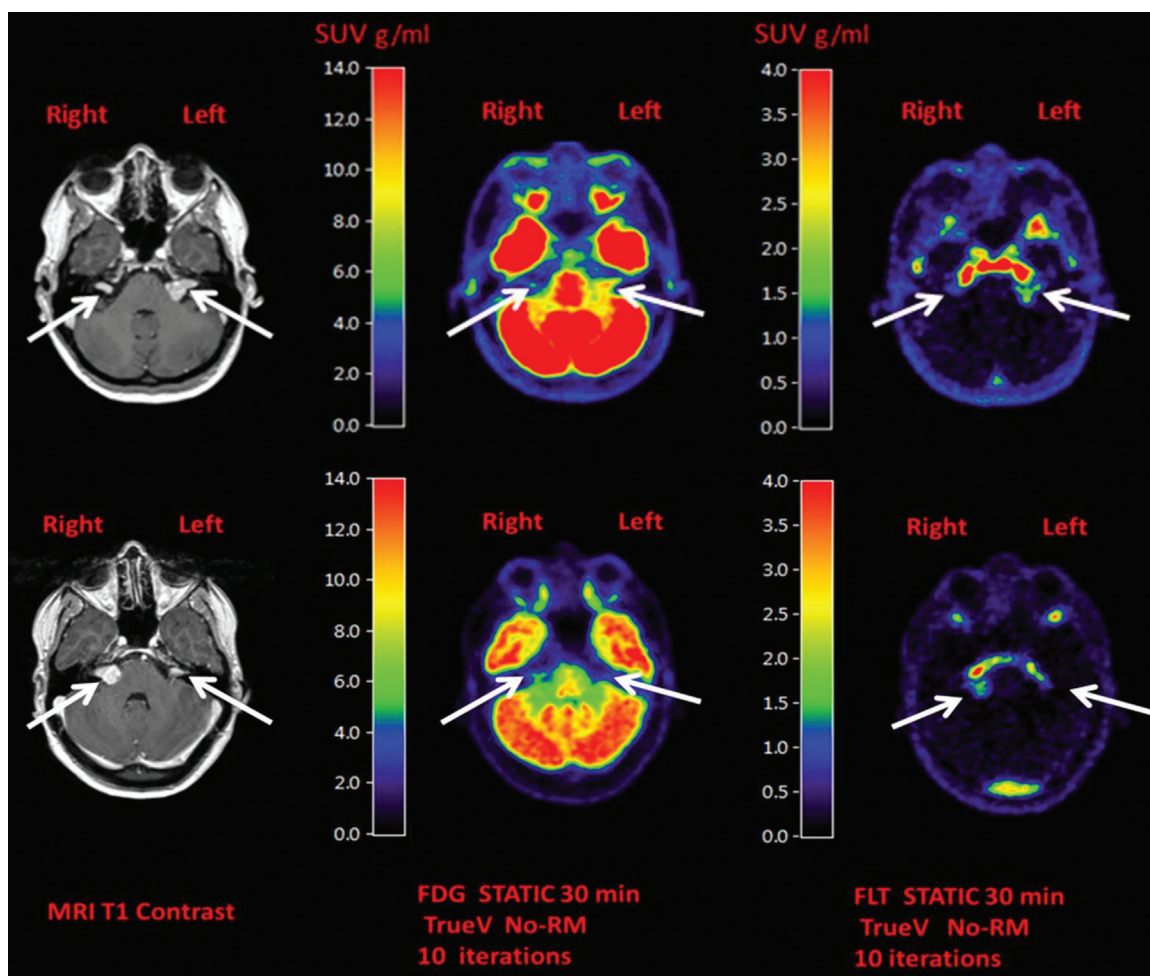


FIG. 1. MRI and FDG/FLT PET images. From left to right: coregistered axial contrast enhanced MRI slices through cerebellopontine angle; axial PET FDG images taken at 30 minutes using TrueV PET-CT scanner without RM; axial PET FLT images taken at 30 minutes using TrueV PET-CT scanner without RM. Top row—33-year-old female (patient A) with bilateral growing VS. High uptake of both FDG and FLT is observed in the larger left-sided VS, with a small area of focal FDG uptake within the right-sided tumor. Bottom row—21-year-old female (patient D) with right-sided growing VS and left-sided slow growing (indolent) tumor. The right lesion shows uptake of both FLT and FDG while the left lesion showed minimal uptake of either tracer. All PET images show the summed activity at approximately 75 to 105 minutes postinjection.

point of the graph represents one of the VS with data shown for the SUV_{mean} with and without RM (rows). Lines of best fit for linear relationships are shown, together with the fit equation and R-squared values. VS classified as rapidly growing are plotted as a solid circle, while indolent tumors are plotted as a square.

Visual inspection of the scatter plots in Figure 3 suggests that FDG and FLT are related to each other in a proportional manner with the use of the higher resolution HRRT scanner and/or RM improving the correlation between FDG and FLT SUV_{mean} values (TrueV: adjusted R^2 value of 0.67 vs 0.73 with RM, HRRT: adjusted R^2 value of 0.85 vs 0.86 with RM). Similar plots for both SUV_{max} and SUV_{peak} without and with RM can be found in supplementary Figures 1C and 2C, <http://links.lww.com/MAO/A784>, for the TrueV and HRRT scanner respectively.

In supplementary Figure 4C, <http://links.lww.com/MAO/A784>, scatter plots of the SUV_{mean} for FDG and FLT versus tumor volume for the TrueV scanner without RM are shown. A weak positive correlation between SUV_{mean} and tumor volume is observed with adjusted R^2 values of 0.18 ($p=0.11$) and 0.08 ($p=0.17$) for FDG and FLT respectively.

Area Under the Curve of the Receiver Operator Characteristic Curve

AUC of the ROC curves for SUV_{mean} , maximum, and peak, for both tracers, and for both scanners are shown in Table 3. Values ranged from 0.714 to 0.857 with SUV_{mean} and from 0.786 to 0.821 with SUV_{peak} , suggesting a good ability of FDG and FLT SUV values to discriminate indolent from rapidly growing tumors. Use of RM for both scanners generally increased the AUC

TABLE 2. Intertumor comparison of derived mean, maximum, and peak SUV values (g/ml) between slow growing (indolent) and fast growing tumors following the injection of FDG and FLT

FDG—Intragroup Mean (+/S.D)		TrueV No-RM			TrueV RM			HRRT No-RM			HRRT RM		
		SUV Mean	SUV Max	SUV Peak	SUV Mean	SUV Max	SUV Peak	SUV Mean	SUV Max	SUV Peak	SUV Mean	SUV Max	SUV Peak
N													
Slow growing (indolent)	7	2.11 (0.88)	4.74 (1.90)	2.57 (1.01)	2.01 (0.94)	4.42 (2.09)	2.56 (1.25)	1.81 (0.87)	10.58 (5.04)	2.28 (1.07)	1.71 (1.00)	5.42 (3.25)	2.19 (1.27)
Fast growing	4	3.49 (1.26)	7.21 (2.16)	4.09 (1.50)	3.61 (1.43)	8.40 (3.57)	4.41 (1.82)	2.96 (0.93)	15.00 (3.97)	3.82 (1.21)	2.95 (0.90)	9.00 (2.25)	3.86 (1.18)
<i>p</i> value		<i>p</i> < 0.05	<i>p</i> = 0.08	<i>p</i> < 0.05	<i>p</i> < 0.05	<i>p</i> < 0.05	<i>p</i> < 0.05						
FLT— Intragroup Mean (+/SD)		TrueV No-RM			TrueV RM			HRRT No-RM			HRRT RM		
		SUV Mean	SUV Max	SUV Peak	SUV Mean	SUV Max	SUV Peak	SUV Mean	SUV Max	SUV Peak	SUV Mean	SUV Max	SUV Peak
N													
Slow growing (indolent)	7	0.86 (0.49)	2.47 (1.34)	1.07 (0.60)	0.94 (0.65)	2.47 (1.81)	1.21 (0.83)	0.68 (0.37)	7.36 (3.23)	0.97 (0.47)	0.74 (0.48)	4.39 (3.03)	1.08 (0.67)
Fast growing	4	1.27 (0.37)	3.47 (1.17)	1.63 (0.57)	1.62 (0.39)	4.43 (1.77)	2.13 (0.74)	1.13 (0.39)	10.18 (4.26)	1.61 (0.66)	1.34 (0.39)	7.14 (2.43)	1.92 (0.70)
<i>p</i> value		<i>p</i> = 0.09	<i>p</i> = 0.12	<i>p</i> = 0.08	<i>p</i> < 0.05	<i>p</i> = 0.06	<i>p</i> = 0.05	<i>p</i> < 0.05	<i>p</i> = 0.12	<i>p</i> < 0.05	<i>p</i> < 0.05	<i>p</i> = 0.08	<i>p</i> < 0.05

Displayed data—intragroup mean SUV (SD). All SUV values derived at approximately 75 to 105 minutes postinjection.

values. Overall, FDG displayed higher AUC values than FLT (0.750–0.893 vs 0.643–0.857) with the exception of SUV_{mean} when using the HRRT scanner with RM, where FLT displayed greater discriminatory power (AUC 0.857 vs 0.821). Both FDG and FLT outperformed tumor volume in discriminating between rapidly growing and indolent tumors with AUC_{ROC} value of 0.601.

DISCUSSION

In this pilot study we have demonstrated for the first time that there is uptake of two commercially available PET radiotracers, FDG and FLT, within NF2 related VS and that uptake of these tracers has the potential ability to discriminate rapidly growing VS from more indolent tumors. This was established through a complex study design to elucidate the relative contributions of tracer, noise, and spatial resolution to the PET signal. The data demonstrates, however, that a short PET acquisition with clinically available tracers on a standard scanner can yield clinically relevant information on tumor growth.

The finding of growth-dependant uptake of FDG in NF2 related VS is in clear contrast to previous inconclusive results with FDG seen in sporadic VS (20,21). While differences in experimental design may partly underlie this discordance, greater uptake of FDG within NF2 related VS may also reflect fundamental biological differences between these two tumor groups at both the macroscopic and microscopic level. While sporadic VS are generally found as a single tumor arising from the vestibular nerve at the porus acousticus (38), NF2 related tumors are often multilobulated, originating from multiple sites on both the vestibular and cochlear nerve (26). At the cellular level, NF2 related VS display higher cellularity (27) and greater immunostaining for cellular proliferation indices (e.g., Ki-67, MIB-1) compared with sporadic tumors (28,39). Furthermore, there is evidence that pathophysiological mechanisms other than cellular proliferation such as cyst formation (40,41), intratumoral hemorrhage (42–44), and inflammation (44–47) may play a greater role in the growth of sporadic VS.

While uptake of FDG and FLT represent differing underlying biological processes, the uptake of both these tracers within NF2 related VS was strongly correlated in our study. One interpretation is that the uptake of FDG and FLT relates to a common factor or process such as tumor size or vascularity, but the correlation between tracer uptake and tumor volume was, however, comparatively weaker than the relationship between FDG and FLT uptake itself. Similarly while increased neovascularization within growing tumors may result in greater early tracer delivery (48,49), with the later PET measurements (75–105 min) used in this study these effects would be minimal. As such, the increased uptake of both FLT and FDG seen in this study likely represents that within growing NF2 related VS there is both concurrent cellular proliferation and increased metabolic demand.

Imaging VS with FDG and FLT has been previously viewed as challenging due to the limited spatial

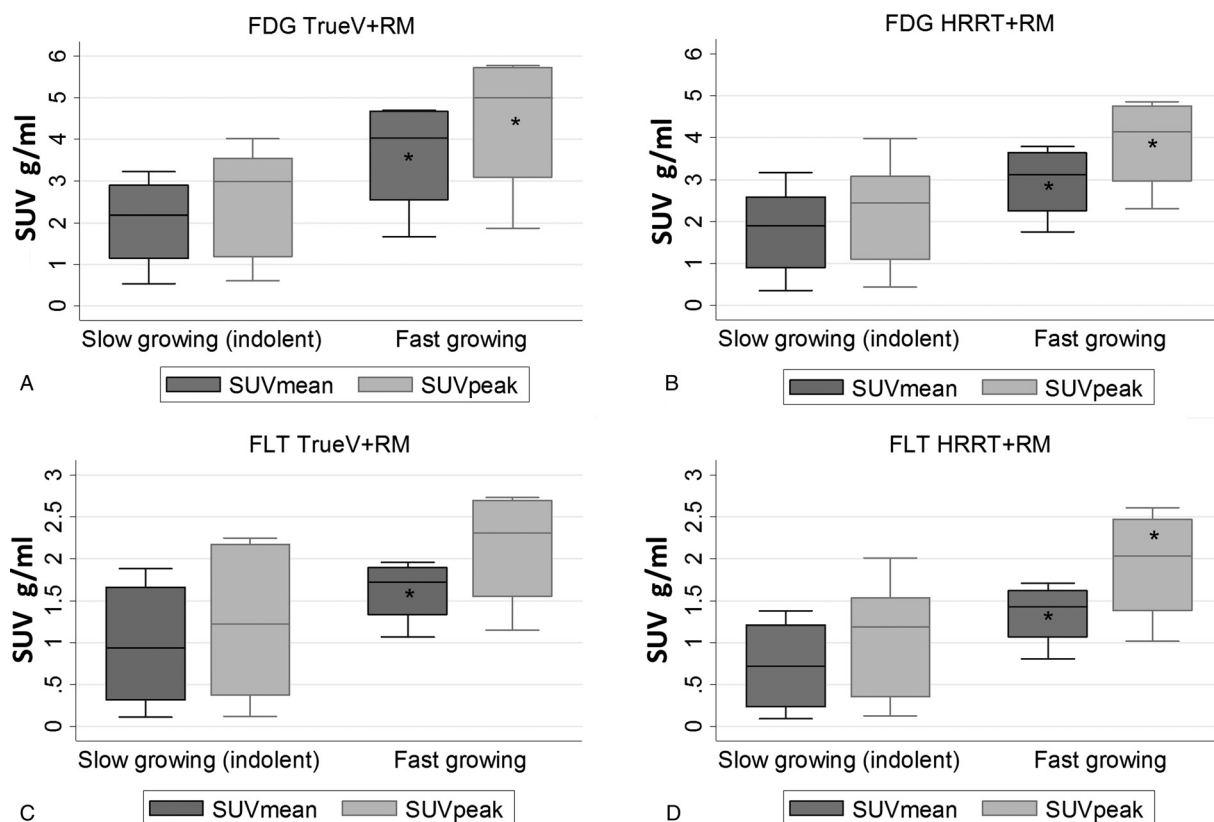


FIG. 2. Intertumor comparison boxplots of derived mean and peak SUV values (g/ml) between slow growing (indolent) and fast growing VS following the injection of FDG and FLT. Using the TrueV PET-CT scanner with RM for FDG (A) and FLT (C); using the HRRT scanner with RM for FDG (B) and FLT (D). * $p < 0.05$ —one tailed Student's t test, comparison between slow growing/indolent and fast growing VS for each SUV parameter.

resolution of conventional PET, leading to potential contamination of tumor uptake from surrounding brain and bony marrow respectively (50). To assess this we used a complex scanning regime which incorporated two different PET scanners with different spatial resolution, both with and without RM reconstruction, and without any postreconstruction image smoothing. One consequence of this approach is that noise in the images is increased and this may explain the reduced discriminatory power of SUV_{max} when compared with SUV_{mean} and SUV_{peak} . Use of either RM or the higher spatial resolution HRRT scanner improved the proportional relationship between FDG and FLT suggesting that when tumor uptake contamination from neighboring tissues is reduced, a better correlation between the two imaged biological processes is observed. Use of the HRRT scanner or RM, however, resulted in only small improvements in AUC_{ROC} values suggesting that the degree of contamination from neighboring structures is small in comparison with the tumor uptake range, and that increased spatial resolution has only a modest effect on tumor growth classification. As such use of more clinically available lower spatial resolution PET scanners such as the TrueV PET-CT scanner may still show good ability to discriminate growing VS.

The results of this study demonstrate that both FDG and FLT uptake has merit to discriminate between rapidly growing and slow growing (indolent) tumors, and that this discriminatory ability exceeds that of tumor volume alone. While standard clinical practice in many institutions is radiological surveillance of tumor growth with serial MRI, there is a danger of missing significant tumor growth between interval scans, with the complication rate and difficulty of surgery increasing as tumors become larger (51,52). In many cases this strategy will be acceptable but select patients exist in whom the ability to predict rather than detect growth may be valuable. The above results suggest that assessment of tumor proliferative and metabolic activity using FDG or FLT PET may have future clinical utility in allowing more timely identification of tumors requiring surgical intervention.

A limitation of this study is that the number of included patients was low, due in part to patient concerns regarding additional radiation exposure and the complexity of the scanning regime. Future, larger studies, which incorporate just one scanner and a single tracer injection of either FDG or FLT, should be performed. These studies could be performed on new generation PET-MR

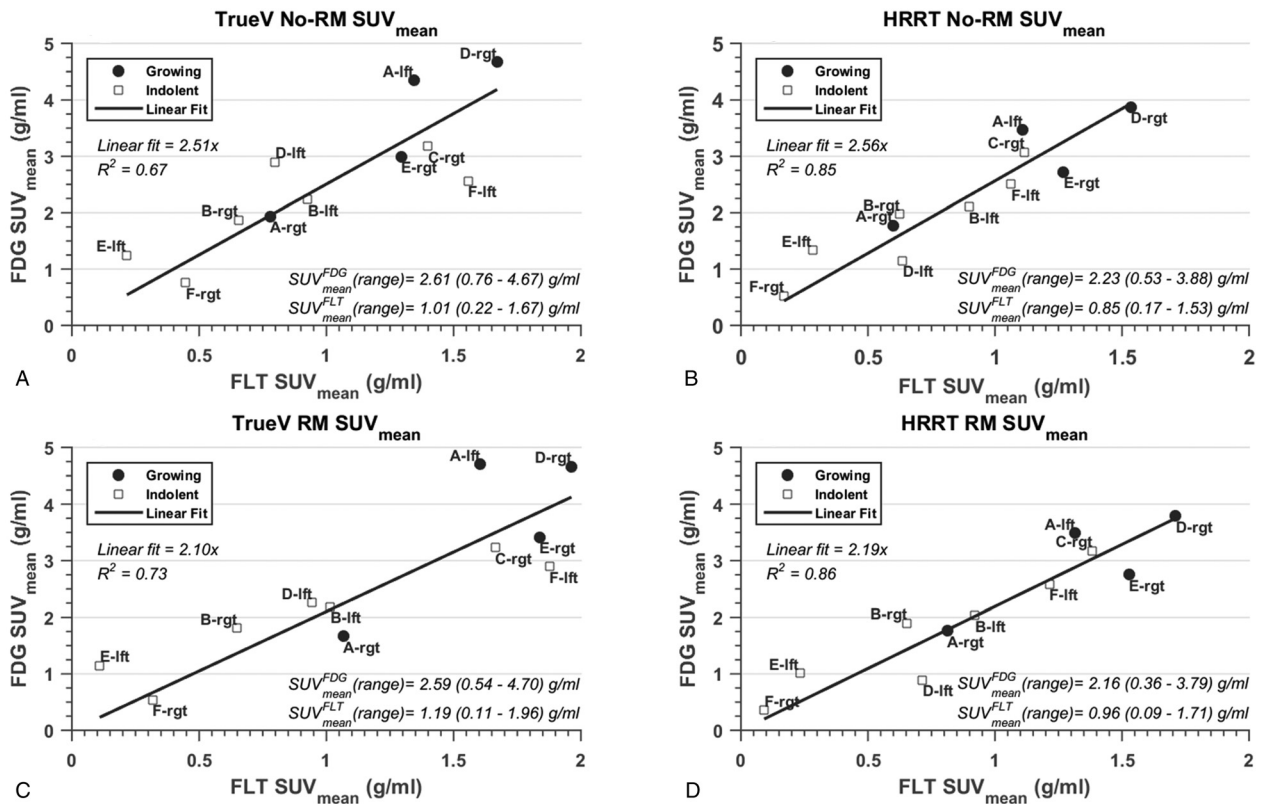


FIG. 3. Intertumor scatterplot comparison of FDG versus FLT uptake. Scatter plots of the mean tumor SUV values of FDG against FLT for both the TrueV (left column) and HRRT scanner (right column) without RM and with RM. For each graph, a line of best fit for proportionality is shown, along with the equation and R² values. Lesions classified as rapid growing (growing) are shown as solid circles, whereas slow growing/indolent lesions are shown as an open square.

scanners, which allow for both simultaneous MR image acquisition and also potentially for reductions in the injected radioactive dose due to improved scanner sensitivity (53). Evaluation of FDG and FLT PET as predictive markers of future tumor growth is limited in part in this study due to loss of growth follow-up in resected tumors. It is, nonetheless, interesting to note that within this study the two non-resected rapidly growing tumors with high FDG and FLT uptake continued to demonstrate rapid growth and larger, prospective studies should be undertaken to further evaluate the role of these tracers as growth predictors.

CONCLUSIONS

Data from 6 NF2 patients, with a total of 11 VS, indicate that for both FLT and FDG an uptake signal above background can be detected and that this uptake shows promise in providing additional and complementary information to serial MRI measurements for the classification of VS which are rapidly growing. Further studies should be undertaken to assess FLT and FDG PET as predictors of tumor growth, and as a clinical imaging tool for early identification of tumors requiring consideration of early treatment.

TABLE 3. Receiver operator characteristic curve (ROC) area under the curve (AUC) values when using volume of lesion (top), and mean, maximum, and peak SUV values (g/ml) of FDG and FLT within contrast enhanced VS lesions to classify lesion growth at approximately 75 to 105 minutes following the injection

Volume Tracer	TrueV No-RM			TrueV RM			HRRT No-RM			HRRT RM		
	SUV Mean	SUV Max	SUV Peak	SUV Mean	SUV Max	SUV Peak	SUV Mean	SUV Max	SUV Peak	SUV Mean	SUV Max	SUV Peak
FDG	0.821	0.786	0.786	0.821	0.821	0.821	0.821	0.750	0.821	0.821	0.893	0.821
FLT	0.714	0.714	0.786	0.821	0.750	0.786	0.786	0.643	0.786	0.857	0.750	0.821
Combined FDG and FLT	0.786	0.821	0.821	0.821	0.821	0.821	0.821	0.679	0.821	0.857	0.857	0.821

Data shown for both the TrueV PET-CT and HRRT PET scanners with and without RM.

Acknowledgments: The authors thank Patricia Braithwaite and Raji Anup for efforts and help in the recruitment of patients at the Highly Specialised Commissioned NF2 service, Central Manchester University Hospital NHS Foundation trust. The authors also thank the staff of the Wolfson Molecular Imaging Centre for help and support to set and run this project, in particular Prof Karl Herholz with his assistance with the ARSAC license and Sarah Wood with the submission of the project to ethics committee.

REFERENCES

- Evans DG, Howard E, Giblin C, et al. Birth incidence and prevalence of tumor-prone syndromes: Estimates from a UK family genetic register service. *Am J Med Genet* 2010;152A:327–32.
- Evans DGR. Neurofibromatosis type 2 (NF2): A clinical and molecular review. *Orphanet J Rare Dis* 2009;4:16.
- Evans DGR, Baser ME, O'Reilly B, et al. Management of the patient and family with neurofibromatosis 2: A consensus conference statement. *Br J Neurosurg* 2005;19:5–12.
- Dirks MS, Butman JA, Kim HJ, et al. Long-term natural history of neurofibromatosis Type 2-associated intracranial tumors. *J Neurosurg* 2012;117:109–17.
- Hexter A, Jones A, Joe H, et al. Clinical and molecular predictors of mortality in neurofibromatosis 2: A UK national analysis of 1192 patients. *J Med Genet* 2015;52:699–705.
- Chen L-H, Zhang H-T, Xu R-X, et al. Microsurgery for patients diagnosed with neurofibromatosis type 2 complicated by vestibular schwannomas: Clinical experience and strategy for treatments. *Medicine* 2018;97:e0270–280.
- Chen L, Chen L, Liu L, et al. Vestibular schwannoma microsurgery with special reference to facial nerve preservation. *Clin Neurol Neurosurg* 2009;111:47–53.
- Nowak A, Dzedzic T, Czernicki T, et al. Strategy for the surgical treatment of vestibular schwannomas in patients with neurofibromatosis type 2. *Neurol Neurochir Pol* 2015;49:295–301.
- Brackmann DE, Fayad JN, Slattery WH 3rd, et al. Early proactive management of vestibular schwannomas in neurofibromatosis type 2. *Neurosurgery* 2001;49:274–80.
- van de Langenberg R, de Bondt BJ, Nelemans PJ, et al. Follow-up assessment of vestibular schwannomas: Volume quantification versus two-dimensional measurements. *Neuroradiology* 2009;51:517–24.
- Harris GJ, Plotkin SR, Maccollin M, et al. Three-dimensional volumetrics for tracking vestibular schwannoma growth in neurofibromatosis type II. *Neurosurgery* 2008;62:1314–9.
- Baser ME, Mautner V-F, Parry DM, et al. Methodological issues in longitudinal studies: Vestibular schwannoma growth rates in neurofibromatosis 2. *J Med Genet* 2005;42:903–6.
- Solares CA, Panizza B. Vestibular schwannoma: An understanding of growth should influence management decisions. *Otol Neurotol* 2008;29:829–34.
- Reivich M, Kuhl D, Wolf A, et al. The [18F]fluorodeoxyglucose method for the measurement of local cerebral glucose utilization in man. *Cir Res* 1979;44:127–37.
- Hsu PP, Sabatini DM. Cancer cell metabolism: Warburg and beyond. *Cell* 2008;134:703–7.
- Warburg O. On the origin of cancer cells. *Science* 1956;123:309–14.
- Endo K, Oriuchi N, Higuchi T, et al. PET and PET/CT using 18F-FDG in the diagnosis and management of cancer patients. *Int J Clin Oncol* 2006;11:286–96.
- Boellaard R, Delgado-Bolton R, Oyen WJG, et al. FDG PET/CT: EANM procedure guidelines for tumour imaging: Version 2.0. *Eur J Nucl Med Mol Imaging* 2015;42:328–54.
- Shields AF, Grierson JR, Dohmen BM, et al. Imaging proliferation in vivo with [F-18]FLT and positron emission tomography. *Nat Med* 1998;4:1334–6.
- Chen JM, Houle S, Ang LC, et al. A study of vestibular schwannomas using positron emission tomography and monoclonal antibody Ki-67. *Am J Otol* 1998;19:840–5.
- Sakamoto H, Nakai Y, Matsuda M, et al. Positron emission tomographic imaging of acoustic neuromas. *Acta Otolaryngol Suppl* 2000;542:18–21.
- Muzi M, Spence AM, O'Sullivan F, et al. Kinetic analysis of 3'-deoxy-3'-18F-fluorothymidine in patients with gliomas. *J Nucl Med* 2006;47:1612–21.
- Schiepers C, Chen W, Dahlbom M, et al. 18F-fluorothymidine kinetics of malignant brain tumors. *Eur J Nucl Med Mol Imaging* 2007;34:1003–11.
- Jacobs AH, Thomas A, Kracht LW, et al. 18F-fluoro-L-thymidine and 11C-methylmethionine as markers of increased transport and proliferation in brain tumors. *J Nucl Med* 2005;46:1948–58.
- Chen W, Cloughesy T, Kamdar N, et al. Imaging proliferation in brain tumors with 18F-FLT PET: Comparison with 18F-FDG. *J Nucl Med* 2005;46:945–52.
- Stivaros SM, Stemmer-Rachamimov AO, Alston R, et al. Multiple synchronous sites of origin of vestibular schwannomas in neurofibromatosis Type 2. *J Med Genet* 2015;52:557–62.
- Sobel RA, Wang Y. Vestibular (Acoustic) schwannomas: Histologic features in neurofibromatosis 2 and in unilateral cases. *J Neuropathol Exp Neurol* 1993;52:106–13.
- Aguiar PH, Tatagiba M, Samii M, et al. The comparison between the growth fraction of bilateral vestibular schwannomas in neurofibromatosis 2 (NF2) and unilateral vestibular schwannomas using the monoclonal antibody MIB 1. *Acta Neurochir* 1995;134:40–5.
- de Jong HW, van Velden FH, Kloet RW, et al. Performance evaluation of the ECAT HRRT: An LSO-LYSO double layer high resolution, high sensitivity scanner. *Phys Med Biol* 2007;52:1505–26.
- Jakoby BW, Bercier Y, Watson CC, et al. Physical performance and clinical workflow of a new LSO HI-REZ PET/CT scanner. *IEEE Nucl Sci Symp Medical Imaging Conf Rec* 2007:3130–4.
- Hudson HM, Larkin RS. Accelerated image reconstruction using ordered subsets of projection data. *IEEE Trans Med Imaging* 1994;13:601–9.
- Panin VY, Kehren F, Michel C, et al. Fully 3-D PET reconstruction with system matrix derived from point source measurements. *IEEE Trans Med Imaging* 2006;25:907–21.
- Comtat C, Sureau FC, Sibomana M, et al. Image based resolution modeling for the HRRT OSEM reconstructions software. *IEEE Nucl Sci Symp Medical Imaging Conf Rec* 2008:4120–3.
- Keller SH, Svarer C, Sibomana M. Attenuation correction for the HRRT PET-scanner using transmission scatter correction and total variation regularization. *IEEE Trans Med Imaging* 2013;32:1611–21.
- Anton-Rodriguez JM, Sibomana M, Walker MD, et al. Investigation of motion induced errors in scatter correction for the HRRT brain scanner. *IEEE Nucl Sci Symp Med Imaging Conf Rec* 2010:2935–40.
- Boellaard R, Krak NC, Hoekstra OS, et al. Effects of noise, image resolution, and ROI definition on the accuracy of standard uptake values: A simulation study. *J Nucl Med* 2004;45:1519–27.
- Wahl RL, Jacene H, Kasamon Y, et al. From RECIST to PERCIST: Evolving considerations for PET response criteria in solid tumors. *J Nucl Med* 2009;50 (suppl 1):122S–50S.
- Neely JG. Gross and microscopic anatomy of the eighth cranial nerve in relationship to the solitary schwannoma. *Laryngoscope* 1981;91:1512–31.
- Antinheimo J, Haapasalo H, Seppala M, et al. Proliferative potential of sporadic and neurofibromatosis 2-associated schwannomas as studied by MIB-1 (Ki-67) and PCNA labeling. *J Neuropathol Exp Neurol* 1995;54:776–82.
- Charabi S, Mantoni M, Tos M, et al. Cystic vestibular schwannomas: Neuroimaging and growth rate. *J Laryngol Otol* 1994;108:375–9.
- Sinha S, Sharma BS. Cystic acoustic neuromas: Surgical outcome in a series of 58 patients. *J Clin Neurosci* 2008;15:511–5.

42. Gomez-Brouchet A, Delisle MB, Cognard C, et al. Vestibular schwannomas: Correlations between magnetic resonance imaging and histopathologic appearance. *Otol Neurotol* 2001;22:79–86.
43. Park CK, Kim DC, Park SH, et al. Microhemorrhage, a possible mechanism for cyst formation in vestibular schwannomas. *J Neurosurg* 2006;105:576–80.
44. de Vries M, Hogendoorn PC, Briaire-de Bruyn I, et al. Intratumoral hemorrhage, vessel density, and the inflammatory reaction contribute to volume increase of sporadic vestibular schwannomas. *Virchows Arch* 2012;460:629–36.
45. Lewis D, Roncaroli F, Agushi E, et al. Inflammation and vascular permeability correlate with growth in sporadic vestibular schwannoma. *Neuro Oncol* 2018. [Epub ahead of print].
46. de Vries M, Briaire-de Bruijn I, Malessy MJ, et al. Tumor-associated macrophages are related to volumetric growth of vestibular schwannomas. *Otol Neurotol* 2013;34:347–52.
47. de Vries M, van der Mey AG, Hogendoorn PC. Tumor biology of vestibular schwannoma: A review of experimental data on the determinants of tumor genesis and growth characteristics. *Otol Neurotol* 2015;36:1128–36.
48. Plotkin SR, Stemmer-Rachamimov AO, Barker FG, et al. Hearing improvement after bevacizumab in patients with neurofibromatosis type 2. *N Engl J Med* 2009;361:358–67.
49. Wong HK, Lahdenranta J, Kamoun WS, et al. Anti-vascular endothelial growth factor therapies as a novel therapeutic approach to treating neurofibromatosis-related tumors. *Cancer Res* 2010;70:3483–93.
50. Soret M, Bacharach SL, Buvat I. Partial-volume effect in PET tumor imaging. *J Nucl Med* 2007;48:932–45.
51. Odat HA, Piccirillo E, Sequino G, et al. Management strategy of vestibular schwannoma in neurofibromatosis type 2. *Otol Neurotol* 2011;32:1163–70.
52. Zhao F, Wang B, Yang Z, et al. Surgical treatment of large vestibular schwannomas in patients with neurofibromatosis type 2: Outcomes on facial nerve function and hearing preservation. *J Neurooncol* 2018;138:417–24.
53. Grant AM, Deller TW, Khalighi MM, et al. NEMA NU 2-2012 performance studies for the SiPM-based ToF-PET component of the GE SIGNA PET/MR system. *Med Phys* 2016;43:2334–43.